Ab initio theory of excitons and optical properties for spin-polarized systems: Application to antiferromagnetic MnO

C. Rödl, F. Fuchs, J. Furthmüller, and F. Bechstedt

Institut für Festkörpertheorie und -optik, Friedrich-Schiller-Universität and European Theoretical Spectroscopy Facility (ETSF), Max-Wien-Platz 1, 07743 Jena, Germany

(Received 10 December 2007; published 6 May 2008)

We study quasiparticle and electron-hole pair excitations in the presence of spin polarization within the framework of many-body perturbation theory. The influence of magnetic ordering on linear optical response is examined in detail for collinear spins. Whereas Hedin's expression for the exchange-correlation self-energy in the *GW* approximation remains diagonal with respect to the one-particle spin quantum number, the Bethe-Salpeter equation becomes more complex: The separation between triplet and singlet excitons no longer holds. The submatrices of the two-particle Hamiltonian are coupled by the matrix elements of the bare Coulomb potential which account for local-field effects. Therefore, the rank of the corresponding eigenvalue problem doubles. Numerical results are computed from first principles for the antiferromagnetic insulator MnO starting from electronic states obtained with nonlocal exchange-correlation potentials. The calculated electronic structure and optical absorption spectra including excitonic and local-field effects are compared with experimental data. The dominance of interatomic transitions between Mn atoms in the interband region of the optical absorption is revealed.

DOI: 10.1103/PhysRevB.77.184408 PACS number(s): 75.10.−b, 71.10.Li, 71.20.Ps, 71.27.+a

I. INTRODUCTION

Recent years have seen impressive methodological progress in accurate numerical modeling of optical properties from first principles using many-body perturbation theory (MBPT).[1] It has become possible to compute one-particle but also two-particle electronic excitations in an accurate manner using Hedin's *GW* approximation (GWA).[2,3] Besides the Dyson equation also the Bethe-Salpeter equation (BSE) for electron-hole pair excitations has been solved in the framework of the same approximation in order to account for excitonic and local-field contributions to the (singlet) polarization function.[4–8] However, the large numerical effort has limited these parameter-free calculations to small systems, such as bulk semiconductors with few atoms in the unit cell[9–11] or simple semiconductor surfaces.[12,13] Recently, this methodology has also been applied to molecular structures.[14–16] In all these applications only spin-paired electrons occur which occupy completely filled electron shells in the ground state. Optical spectra of systems with spin polarization or magnetic ordering have not been studied in the context of MBPT until now.

However, spin-dependent phenomena become more and more important also for nonmetallic materials. This holds for transition-metal oxides[17–19] (TMOs) with antiferromagnetic ordering below the Néel temperature or transition-metal nitrides[20,21] which may be transferred into a ferromagnetic ground state in thin strained layers. One driving force is the development of spintronics,[22] especially after the discovery of ferromagnetic diluted magnetic semiconductors[23,24] in which small amounts of transition metals are incorporated into host semiconductors such as GaAs, GaN, or ZnO. Quasi-one-dimensional systems as metal chains on semiconductor surfaces may show novel spin-dependent phenomena such as a possible spin-charge separation in the electronic excitations.[25,26] Exciton formation and optical excitations in polymer chains of π-conjugated compounds are also found to be spin dependent.[27] Moreover, electronic excitations in molecules containing magnetic ions are influenced by spin polarization.[28]

The antiferromagnetic TMOs, such as MnO and NiO, represent prototypical systems to investigate the influence of spin polarization on many-body effects in optical spectra, in particular the electron-hole interaction. These oxides have small primitive unit cells containing only four atoms. They are insulators with not too small gaps and hence not too strong electronic screening of the electron-hole attraction. The TMOs show an antiferromagnetic ordering of the transition-metal spins due to their partially filled 3*d* shells. Because of the high localization of the *d* states, strong Coulomb correlation may occur in these systems. Consequently, this class of materials represents typical Mott insulators.[17–19] Their treatment is accompanied by difficulties to deal correctly with the ground-state properties and the electronic structure.[29,30] Especially, conventional density functional theory (DFT) with a local or semilocal description of the exchange-correlation (XC) energy functional within the local spin density approximation (LSDA) or generalized gradient approximation (GGA) with spin polarization are known to be inadequate to account for the electronic structure of materials with localized *d* orbitals. Different ways have been suggested to overcome the mentioned deficiencies of the (semi)local approaches. One is to include a self-interaction correction (SIC).[31] In another approach, the so-called LDA (GGA) $+U$ method,[18,30,32] an orbital-dependent correction is added to the LDA (GGA) XC potential. Further, the spatial nonlocality of exchange and correlation can be partially accounted for by a hybrid functional approach.[30] Meanwhile, one-particle electronic excitations and band structures of MnO and NiO have also been treated within the quasiparticle (QP) approach using the GWA for the XC self-energy.[19,33–35] Recently, a new approach to the electronic structure of strongly

correlated materials has been developed, the dynamical mean-field theory.[36] Its self-consistent implementation has been shown to be directly related to Hedin's *GW* perturbation theory.[37]

In the present paper we investigate electron-hole pair excitations with spin polarization within the framework of MBPT. In Sec. II the theoretical framework is developed. We study Hedin's equations for systems with magnetic ordering and derive the BSE for the polarization function in the case of noncollinear spins. The BSE is solved in the limit of collinear spin polarization.

Numerical results for excitonic effects and optical absorption spectra are presented for the antiferromagnetic insulator MnO. We consider the paradigmatic case of MnO, since the Mn^{2+} ion possesses a half-filled shell ($3d^5$) with maximum total spin according to Hund's rule and spin subbands which are either completely filled or empty.

For the calculations we apply DFT[38] within the GGA in order to obtain the structurally relaxed ground-state configuration with magnetic ordering. The Kohn-Sham[39] (KS) eigenvalues and eigenfunctions allow for a representation of the one- and two-particle Green's functions whose poles define the respective excitation energies. The resulting electronic band structure of MnO is discussed in Sec. III. DFT with the nonlocal HSE03 (Ref. 40) XC functional is utilized to provide a better starting point for the calculation of the electronic QP spectrum. The latter is obtained within the GWA for the XC self-energy.[41,42] The large number of **k** points required for the calculation of optical spectra necessitates a computationally less expensive way to generate QP energies. Therefore, we calculate the QP electronic structure also in a simplified scheme based on GGA+U and the scissors-operator approach,[42] which, however, widely reproduces the results of the more sophisticated approach.

Finally, in Sec. IV we calculate optical spectra and examine excitonic as well as spin effects in these spectra. The BSE, which becomes a matrix equation in spin space in the presence of spin polarization, is solved, taking into account the screened electron-hole attraction and the bare electron-hole exchange term. The results are discussed and compared with available experimental data.

II. THEORETICAL APPROACHES

A. Fundamental system of equations

In order to address the problem of solving the BSE for magnetic materials we derive the basic equations of MBPT with special attention to effects arising from the inclusion of spin polarization. For systems with noncollinear spins the many-body Hamiltonian can be divided into three contributions,

$$\hat{H} = \hat{T} + \hat{V} + \hat{U}. \tag{1}$$

Besides the one-particle operator of the kinetic energy,

$$\hat{T} = \sum_{s} \int d\mathbf{r}\ \psi_s^\dagger(\mathbf{r}) \left(-\frac{\hbar^2}{2m_0}\Delta \right) \psi_s(\mathbf{r}), \tag{2}$$

with the creation operator $\psi_s^\dagger(\mathbf{r})$ and the annihilation operator $\psi_s(\mathbf{r})$ for an electron with spin variable s at the point $\mathbf{r}$ in real space, an external potential is considered which is generally not diagonal with respect to the spin variables and contains a magnetic field and the spin-orbit coupling term,

$$\hat{V} = \sum_{ss'} \int d\mathbf{r}\ \psi_s^\dagger(\mathbf{r}) V_{ss'}(\mathbf{r}) \psi_{s'}(\mathbf{r}), \tag{3}$$

$$V_{ss'}(\mathbf{r}) = V(\mathbf{r})\delta_{ss'} + \mu_B \boldsymbol{\sigma}_{ss'} \cdot \left(\mathbf{B}(\mathbf{r}) + \frac{\nabla V(\mathbf{r}) \times \mathbf{p}}{2em_0c^2} \right). \tag{4}$$

Here, $V(\mathbf{r})$ represents a scalar external potential, while $\boldsymbol{\sigma}_{ss'}$ denotes the vector of Pauli matrices. Magnetism is treated in the nonrelativistic limit. More precisely, a Pauli term proportional to the magnetic field $\mathbf{B}(\mathbf{r})$ is included, whereas additional contributions arising from the vector potential are neglected. The limit of collinear spin polarization is obtained if $\mathbf{B}(\mathbf{r})$ has a fixed direction which can be labeled z without loss of generality. The electron-electron interaction

$$\hat{U} = \frac{1}{2}\sum_{ss'} \int d\mathbf{r} \int d\mathbf{r}'\ \psi_{s'}^\dagger(\mathbf{r}') \psi_s^\dagger(\mathbf{r}) v(\mathbf{r}-\mathbf{r}') \psi_s(\mathbf{r}) \psi_{s'}(\mathbf{r}'), \tag{5}$$

with the Coulomb potential $v(\mathbf{r}-\mathbf{r}') = e^2/4\pi\varepsilon_0|\mathbf{r}-\mathbf{r}'|$, is described in the longitudinal approach, while current-induced effects and spin-spin coupling are neglected.

Introducing the abbreviation $1 = \mathbf{r}_1 t_1$ for spatial and time coordinate, the time-ordered one-particle Green's function of the N-particle system is defined by

$$G\left(\begin{smallmatrix} 1 & 2 \\ s_1 & s_2 \end{smallmatrix}\right) = \frac{1}{i\hbar}\langle N|T\psi_{s_1}(1)\psi_{s_2}^\dagger(2)|N\rangle, \tag{6}$$

whereas T denotes the time-ordering symbol and $|N\rangle$ the N-particle ground state. The Green's function fulfills the Dyson equation of motion

$$\sum_{s_3} \left[\left(i\hbar\frac{\partial}{\partial t_1} + \frac{\hbar^2}{2m_0}\Delta_{\mathbf{r}_1} - V_H(\mathbf{r}_1) \right) \delta_{s_1 s_3} - V_{s_1 s_3}(\mathbf{r}_1) \right] G\left(\begin{smallmatrix} 1 & 2 \\ s_3 & s_2 \end{smallmatrix}\right)$$
$$- \sum_{s_3} \int d3\ \Sigma\left(\begin{smallmatrix} 1 & 3 \\ s_1 & s_3 \end{smallmatrix}\right) G\left(\begin{smallmatrix} 3 & 2 \\ s_3 & s_2 \end{smallmatrix}\right) = \delta(1-2)\delta_{s_1 s_2}, \tag{7}$$

with the Hartree potential $V_H(\mathbf{r}) = \int d\mathbf{r}'\ v(\mathbf{r}-\mathbf{r}')n(\mathbf{r}')$ which is only determined by the electron density $n(\mathbf{r})$. Therefore, the Hartree potential is spin independent. In contrast to the Hartree potential the XC self-energy Σ, which obeys the equation

$$\Sigma\left(\begin{smallmatrix} 1 & 2 \\ s_1 & s_2 \end{smallmatrix}\right) = -\sum_{s_3 s_4} \int d(34) v(1-3)$$
$$\times L\left(\begin{smallmatrix} 1 & 4 \\ s_1 & s_4 \end{smallmatrix} \middle| \begin{smallmatrix} 3 & 3^+ \\ s_3 & s_3 \end{smallmatrix}\right) G^{-1}\left(\begin{smallmatrix} 4 & 2 \\ s_4 & s_2 \end{smallmatrix}\right), \tag{8}$$

depends on the spin variables. The superscript 3^+ stands for

an infinitesimal shift of the time coordinate to keep the correct time ordering. The self-energy can be expressed by means of the density-density correlation function

$$L\left(\begin{smallmatrix}1&1'\\s_1&s_1'\end{smallmatrix}\middle|\begin{smallmatrix}2&2'\\s_2&s_2'\end{smallmatrix}\right)=i\hbar\left[G\left(\begin{smallmatrix}1&2\\s_1&s_2\end{smallmatrix}\middle|\begin{smallmatrix}1'&2'\\s_1'&s_2'\end{smallmatrix}\right)-G\left(\begin{smallmatrix}1&1'\\s_1&s_1'\end{smallmatrix}\right)G\left(\begin{smallmatrix}2&2'\\s_2&s_2'\end{smallmatrix}\right)\right], \quad (9)$$

which contains the two-particle Green's function

$$G\left(\begin{smallmatrix}1&2\\s_1&s_2\end{smallmatrix}\middle|\begin{smallmatrix}1'&2'\\s_1'&s_2'\end{smallmatrix}\right)=\frac{1}{(i\hbar)^2}\langle N|T\psi_{s_1}(1)\psi_{s_2}(2)\psi^\dagger_{s_2'}(2')\psi^\dagger_{s_1'}(1')|N\rangle \quad (10)$$

and the product of two single-particle Green's functions.

We consider a vanishingly small external perturbation $U^{test}_{ss'}(\mathbf{r})$, which also comprises a magnetic contribution,

$$U^{test}_{ss'}(\mathbf{r})=V^{test}(\mathbf{r})\delta_{ss'}+\mu_B\boldsymbol{\sigma}_{ss'}\cdot\mathbf{B}^{test}(\mathbf{r}). \quad (11)$$

Applying the method of variational derivatives and assuming that $U^{test}_{ss'}(\mathbf{r})$ does not induce any phase transition with respect to the initial Hamiltonian (1), we find Hedin's equations for a magnetic system which account for the noncollinear spin structure. The self-energy in the Dyson equation (7) can be expressed by means of

$$\Sigma\left(\begin{smallmatrix}1&2\\s_1&s_2\end{smallmatrix}\right)=-i\hbar\sum_{s_3s_4}\int d(34)G\left(\begin{smallmatrix}1&3\\s_1&s_3\end{smallmatrix}\right)\Gamma\left(\begin{smallmatrix}3&2\\s_3&s_2\end{smallmatrix}\middle|\begin{smallmatrix}4\\s_4\end{smallmatrix}\right)W(1^+4), \quad (12)$$

with the dynamically screened Coulomb potential

$$W(12)=v(1-2)+\sum_{s_3s_4}\int d(34)v(1-3)P\left(\begin{smallmatrix}3&4\\s_3&s_4\end{smallmatrix}\right)W(42). \quad (13)$$

The screened potential is governed by the irreducible polarization function

$$P\left(\begin{smallmatrix}1&2\\s_1&s_2\end{smallmatrix}\right)=-\sum_{s_3s_4}\int d(34)L_0\left(\begin{smallmatrix}1&1^+\\s_1&s_1\end{smallmatrix}\middle|\begin{smallmatrix}4&3\\s_4&s_3\end{smallmatrix}\right)\Gamma\left(\begin{smallmatrix}3&4\\s_3&s_4\end{smallmatrix}\middle|\begin{smallmatrix}2\\s_2\end{smallmatrix}\right), \quad (14)$$

with the independent-particle polarizability

$$L_0\left(\begin{smallmatrix}1&1'\\s_1&s_1'\end{smallmatrix}\middle|\begin{smallmatrix}2&2'\\s_2&s_2'\end{smallmatrix}\right)=-i\hbar G\left(\begin{smallmatrix}1&2'\\s_1&s_2'\end{smallmatrix}\right)G\left(\begin{smallmatrix}2&1'\\s_2&s_1'\end{smallmatrix}\right). \quad (15)$$

The vertex function Γ is determined by a BSE of the form

$$\Gamma\left(\begin{smallmatrix}1&2\\s_1&s_2\end{smallmatrix}\middle|\begin{smallmatrix}3\\s_3\end{smallmatrix}\right)=-\delta(1-2)\delta(1-3)\delta_{s_1s_2}\delta_{s_1s_3}+\sum_{s_4s_5s_6s_7}\int d(4567)\,\Xi\left(\begin{smallmatrix}1&2\\s_1&s_2\end{smallmatrix}\middle|\begin{smallmatrix}4&5\\s_4&s_5\end{smallmatrix}\right)\times L_0\left(\begin{smallmatrix}4&5\\s_4&s_5\end{smallmatrix}\middle|\begin{smallmatrix}7&6\\s_7&s_6\end{smallmatrix}\right)\Gamma\left(\begin{smallmatrix}6&7\\s_6&s_7\end{smallmatrix}\middle|\begin{smallmatrix}3\\s_3\end{smallmatrix}\right), \quad (16)$$

whose kernel

$$\Xi\left(\begin{smallmatrix}1&2\\s_1&s_2\end{smallmatrix}\middle|\begin{smallmatrix}3&4\\s_3&s_4\end{smallmatrix}\right)=-\frac{1}{i\hbar}\delta\Sigma\left(\begin{smallmatrix}1&2\\s_1&s_2\end{smallmatrix}\right)\Big/\delta G\left(\begin{smallmatrix}3&4\\s_3&s_4\end{smallmatrix}\right) \quad (17)$$

equates the functional derivative of the self-energy with respect to the Green's function. Inserting (16) into (14) yields a BSE for the irreducible polarization function,

$$P\left(\begin{smallmatrix}1&1'\\s_1&s_1'\end{smallmatrix}\middle|\begin{smallmatrix}2&2'\\s_2&s_2'\end{smallmatrix}\right)=L_0\left(\begin{smallmatrix}1&1'\\s_1&s_1'\end{smallmatrix}\middle|\begin{smallmatrix}2&2'\\s_2&s_2'\end{smallmatrix}\right)+\sum_{\substack{s_3s_4\\s_5s_6}}\int d(3456)\,L_0\left(\begin{smallmatrix}1&1'\\s_1&s_1'\end{smallmatrix}\middle|\begin{smallmatrix}4&3\\s_4&s_3\end{smallmatrix}\right)\times\Xi\left(\begin{smallmatrix}3&4\\s_3&s_4\end{smallmatrix}\middle|\begin{smallmatrix}5&6\\s_5&s_6\end{smallmatrix}\right)P\left(\begin{smallmatrix}5&6\\s_5&s_6\end{smallmatrix}\middle|\begin{smallmatrix}2&2'\\s_2&s_2'\end{smallmatrix}\right). \quad (18)$$

This four-point quantity is related to the two-point polarization function by

$$P\left(\begin{smallmatrix}1&2\\s_1&s_2\end{smallmatrix}\right)=P\left(\begin{smallmatrix}1&1^+\\s_1&s_1\end{smallmatrix}\middle|\begin{smallmatrix}2&2^+\\s_2&s_2\end{smallmatrix}\right). \quad (19)$$

For reasons of clarity the spin variables are explicitly denoted wherever they appear in the formulas. As one can see, the bare Coulomb potential and its screened counterpart are the only quantities that do not explicitly depend on spin. The consequences of this observation will be discussed in more detail below.

B. Relation to optical response

Optical response properties as well as the dynamically screened Coulomb potential W depend on the microscopic dielectric function ε or its inverse ε^{-1}, respectively. For the screened potential the relation

$$W(12)=\int d3\, v(1-3)\varepsilon^{-1}(23) \quad (20)$$

holds. It has to be stressed that W and ε^{-1} are spin-independent quantities. Considering the two-point counterpart of the density-density correlation function (9), which is defined analogously to (19), the explicit expression

$$\varepsilon^{-1}(12)=\delta(1-2)+\sum_{s_2s_3}\int d3\, v(1-3)L\left(\begin{smallmatrix}3&2\\s_3&s_2\end{smallmatrix}\right) \quad (21)$$

for the inverse dielectric function is derived. At this point it is important to note that the sum has to be taken over both spin variables s_2 and s_3, while the integral only runs over one spatial and time coordinate. This equation is crucial for the treatment of spin in the framework of MBPT. It shows that the space- and time-dependent dielectric response is determined by the contributions from all electrons, no matter what the values of their spin variables are. Inverting the last equation results in an expression for the microscopic dielectric function,

$$\varepsilon(12)=\delta(1-2)-\sum_{s_2s_3}\int d3\, v(1-3)P\left(\begin{smallmatrix}3&2\\s_3&s_2\end{smallmatrix}\right), \quad (22)$$

which is governed by the irreducible polarization function (14) and, once again, contains a sum over all spin variables.

The transition from microscopic dielectric response to macroscopic optics is performed by a spatial averaging procedure according to Adler[43] and Wiser.[44] In the optical limit of vanishing wave vector $\mathbf{q}\to 0$ the Fourier transform of the macroscopic dielectric function for a translationally invariant system can be obtained according to

$$\varepsilon_{mac}(\hat{\mathbf{q}},\omega) = \lim_{\mathbf{q}\to 0} \left. \frac{1}{\varepsilon^{-1}(\mathbf{q}+\mathbf{G},\mathbf{q}+\mathbf{G}',\omega)} \right|_{\mathbf{G}=\mathbf{G}'=0}. \quad (23)$$

Henceforth, the wave vector $\mathbf{q}$ runs over the Brillouin zone (BZ), while $\mathbf{G}$ and $\mathbf{G}'$ denote elements of the reciprocal Bravais lattice. The unit vector in the direction of light incidence is labeled $\hat{\mathbf{q}}=\mathbf{q}/|\mathbf{q}|$. The off-diagonal elements $\mathbf{G}\neq\mathbf{G}'$ of the inverse dielectric matrix describe local-field effects (LFEs)—i.e., the differences between microscopic and macroscopic electric fields in the system. The consequences of Eq. (23) for the kernel in the BSE of the corresponding macroscopic polarization function will be discussed below.

C. Random-phase approximation for collinear spins

The restriction to collinear spin polarization allows for substantial simplifications of the formalism. This is demonstrated here for the dielectric function in random-phase approximation (RPA). Within the scope of collinear magnetism the one-particle wave functions, which are in general two-component spinors, can be split into a spin and a spatial part according to

$$\xi_\lambda^m\left(\begin{matrix}\mathbf{r}\\ s\end{matrix}\right) = \eta_m(s)\varphi_\lambda^m(\mathbf{r}),$$

whereas the latter depends parametrically on the spin quantum number $m=\uparrow,\downarrow$. The spinors $\eta_m(s)$ constitute the basis in one-particle spin space. For reasons of conciseness the band index and the $\mathbf{k}$ point are labeled by a single spatial quantum number λ. The spatial eigenfunctions $\varphi_\lambda^m(\mathbf{r})=\langle\mathbf{r}|\lambda m\rangle$ as well as the corresponding eigenvalues ε_λ^m are calculated in a KS scheme,[39] thus solving the equation

$$\left[-\frac{\hbar^2}{2m_0}\Delta + V^m(\mathbf{r}) + V_H(\mathbf{r}) + V_{XC}^m(\mathbf{r})\right]\varphi_\lambda^m(\mathbf{r}) = \varepsilon_\lambda^m\varphi_\lambda^m(\mathbf{r}) \quad (24)$$

self-consistently with the density-dependent XC potential V_{XC}^m. The corresponding Green's function of independent KS particles in Bloch-Fourier representation becomes diagonal in spin space with diagonal elements,

$$G^m(\mathbf{r}\mathbf{r}',\omega) = \sum_\lambda \frac{\varphi_\lambda^m(\mathbf{r})\varphi_\lambda^{*m}(\mathbf{r}')}{\hbar\omega-\varepsilon_\lambda^m}, \quad (25)$$

which are determined by the contributions of spin-up and spin-down electrons, respectively.

The frequency-dependent dielectric function in the optical limit results from a Fourier transform of Eq. (22),

$$\varepsilon(\mathbf{q},\omega) = 1 - \frac{1}{\Omega}\frac{e^2}{\varepsilon_0|\mathbf{q}|^2}\sum_{m_1m_2}\sum_{\lambda_1\lambda_1'\lambda_2\lambda_2'}\langle\lambda_1 m_1|e^{i\mathbf{q}\cdot\mathbf{r}}|\lambda_1' m_1\rangle^* \times\langle\lambda_2' m_2|e^{i\mathbf{q}\cdot\mathbf{r}}|\lambda_2 m_2\rangle P\left(\begin{matrix}\lambda_1 & \lambda_1'\\ m_1 & m_1\end{matrix}\middle|\begin{matrix}\lambda_2 & \lambda_2'\\ m_2 & m_2\end{matrix}\middle|\omega\right). \quad (26)$$

Here, the crystal volume is labeled by Ω. In the case of the RPA the polarization function P has to be approximated by the independent-particle polarizability (15). Due to the spin selection rule, only such optical transitions where the spin quantum number in the valence and conduction band does not change contribute to the absorption in collinear spin-polarized systems. Other transitions are dipole forbidden. In the limit of vanishing $\mathbf{q}$ the transition matrix elements between filled valence bands v and empty conduction bands c can be evaluated by means of the velocity operator

$$\langle c\mathbf{k}m|e^{i\mathbf{q}\cdot\mathbf{r}}|v\mathbf{k}m\rangle = \frac{\hbar|\mathbf{q}|}{m_0}\frac{\langle c\mathbf{k}m|\hat{\mathbf{q}}\cdot\mathbf{p}|v\mathbf{k}m\rangle}{\varepsilon_{c\mathbf{k}}^m-\varepsilon_{v\mathbf{k}}^m}, \quad (27)$$

whereas $\mathbf{p}$ denotes the momentum operator. By introducing a broadening γ to circumvent the singularities in the complex plane one ends up with

$$\varepsilon^{\alpha\alpha}(\omega) = 1 + \frac{1}{\Omega}\frac{e^2\hbar^2}{\varepsilon_0 m_0^2}\sum_{cv\mathbf{k}m}\left|\frac{\langle c\mathbf{k}m|p_\alpha|v\mathbf{k}m\rangle}{\varepsilon_{c\mathbf{k}}^m-\varepsilon_{v\mathbf{k}}^m}\right|^2 \times\sum_{\beta=\pm1}\frac{1}{\varepsilon_{c\mathbf{k}}^m-\varepsilon_{v\mathbf{k}}^m-\beta\hbar(\omega+i\gamma)} \quad (28)$$

for the microscopic dielectric function in the Cartesian direction α. It has to be stressed that, in line with the one-particle spin selection rule, this equation obviously does not contain any contributions to optical absorption which arise from spin-flip processes. This is reasonable as in the framework of collinear spin polarization any mechanisms that could flip spins are absent. Such mechanisms could be a coupling of orbital motion with spin or the influence of noncollinear magnetization. For the collinear spin-polarized case Eq. (28) shows that one simply has to sum over the contributions from spin-up and spin-down electrons which can be calculated independently.

D. Hedin's *GW* approximation

As the computational costs for solving Hedin's equations self-consistently for any condensed-matter system are prohibitively large, approximations are necessary. Within the *GW* approach the vertex function (16) is approximated by the contribution arising from the δ function. For the self-energy (12) this implies

$$\Sigma\left(\begin{matrix}1 & 2\\ s_1 & s_2\end{matrix}\right) = i\hbar G\left(\begin{matrix}1 & 2\\ s_1 & s_2\end{matrix}\right)W(1^+2). \quad (29)$$

On this level of approximation the spin dependence of the self-energy is completely ruled by the spin dependence of the Green's function. This is particularly convenient in the limit of collinear spins where the Green's function is diagonal in spin space [see Eq. (25)] and the self-energy for spin-up and spin-down electrons can be calculated independently. Nevertheless, it should be kept in mind that the screening in W has to be evaluated in RPA by adding up the contributions from all electrons.

Starting from the Dyson equation (7) one can derive a QP equation[3]

$$\left[\frac{\mathbf{p}^2}{2m_0} + V^m + V_H + \Sigma^m(E_\lambda^m)\right]|\phi_\lambda^m\rangle = E_\lambda^m|\phi_\lambda^m\rangle, \quad (30)$$

whose solutions are the one-particle wave functions $|\phi_\lambda^m\rangle$ and energy eigenvalues E_λ^m of the QP excitations. Assuming that $|\phi_\lambda^m\rangle\approx|\lambda m\rangle$ holds,[41] the QP eigenvalues can be determined in first-order perturbation theory on top of the KS results (the so-called G_0W_0 approach) using

$$E_\lambda^m = \varepsilon_\lambda^m + Z_\lambda^m \,\mathrm{Re}\langle \lambda m|\Sigma^m(\varepsilon_\lambda^m) - V_{XC}^m|\lambda m\rangle, \tag{31}$$

with the QP renormalization factor

$$Z_\lambda^m = \left(1 - \mathrm{Re}\langle \lambda m| \left.\frac{\partial \Sigma^m(\varepsilon)}{\partial \varepsilon}\right|_{\varepsilon=\varepsilon_\lambda^m} |\lambda m\rangle\right)^{-1}. \tag{32}$$

E. Electron-hole excitations for collinear spins

Including electron-hole interaction in the calculation of optical properties means going beyond the RPA, thus considering a nonvanishing kernel Ξ in the BSE (18). Following the concept of iterating Hedin's equations the self-energy which enters the kernel (17) is approximated in the *GW* approximation [see Eq. (29)]. Subsequently, the functional derivative is carried out, whereas the variation of W with respect to G is neglected.[7] Hanke and Sham[5,6] have demonstrated that it is possible to derive a BSE for a generalized polarization function $\bar{P}$ which directly yields ε_{mac} in analogy to Eq. (22) and circumvents the inversion procedure (23). In the kernel

$$\bar{\Xi}\left(\begin{smallmatrix} 1 & 2 \\ s_1 & s_2 \end{smallmatrix}\middle|\begin{smallmatrix} 3 & 4 \\ s_3 & s_4 \end{smallmatrix}\right) = -\,\delta(1-3)\,\delta_{s_1 s_3}\,\delta(2-4)\,\delta_{s_2 s_4} W(1^+2) + \delta(1-2)\,\delta_{s_1 s_2}\,\delta(3^+-4)\,\delta_{s_3 s_4}\bar{v}(1-3) \tag{33}$$

of the BSE for $\bar{P}$ the bare Coulomb potential $\bar{v}$ appears additionally to the screened electron-hole attraction W. Thereby, the overbar signifies that the exchange term v has to be taken without its long-range Fourier component $\mathbf{G}=0$. The occurrence of the dynamically screened Coulomb potential in the kernel prohibits the formulation of a closed BSE[7] for $\bar{P}$ depending on only one frequency ω. Thus, the dynamics of screening is neglected and only the static screening $W(\mathbf{r},\mathbf{r}')\delta(t-t')$ is considered.

For semiconductors and insulators, whose bands are either completely filled or empty, the BSE (18) with the kernel (33) can be rewritten as an eigenvalue problem for an effective two-particle Hamiltonian H_{exc},

$$\sum_{m_c' m_v'} \sum_{c' v' \mathbf{k}'} H_{exc}\left(\begin{smallmatrix} c\mathbf{k} & v\mathbf{k} \\ m_c & m_v \end{smallmatrix}\middle|\begin{smallmatrix} c'\mathbf{k}' & v'\mathbf{k}' \\ m_c' & m_v' \end{smallmatrix}\right) A_\Lambda\left(\begin{smallmatrix} c'\mathbf{k}' & v'\mathbf{k}' \\ m_c' & m_v' \end{smallmatrix}\right) = E_\Lambda A_\Lambda\left(\begin{smallmatrix} c\mathbf{k} & v\mathbf{k} \\ m_c & m_v \end{smallmatrix}\right). \tag{34}$$

In this Hamiltonian the coupling between resonant and antiresonant contributions as well as interaction matrix elements that do not conserve the particle numbers are usually neglected. The solution of the eigenvalue problem determines the spectral representation of the four-point polarization function,

$$\bar{P}\left(\begin{smallmatrix} c\mathbf{k} & v\mathbf{k} \\ m_c & m_v \end{smallmatrix}\middle|\begin{smallmatrix} v'\mathbf{k}' & c'\mathbf{k}' \\ m_v' & m_c' \end{smallmatrix}\middle|\,\omega\right) = \sum_\Lambda \frac{A_\Lambda\left(\begin{smallmatrix} c\mathbf{k} & v\mathbf{k} \\ m_c & m_v \end{smallmatrix}\right) A_\Lambda^*\left(\begin{smallmatrix} c'\mathbf{k}' & v'\mathbf{k}' \\ m_c' & m_v' \end{smallmatrix}\right)}{\hbar\omega - E_\Lambda}. \tag{35}$$

The so-called excitonic or pair Hamiltonian

$$\begin{aligned} H_{exc}&\left(\begin{smallmatrix} c\mathbf{k} & v\mathbf{k} \\ m_c & m_v \end{smallmatrix}\middle|\begin{smallmatrix} c'\mathbf{k}' & v'\mathbf{k}' \\ m_c' & m_v' \end{smallmatrix}\right) \\ &= +(E_{c\mathbf{k}}^{m_c} - E_{v\mathbf{k}}^{m_v})\,\delta_{cc'}\,\delta_{vv'}\,\delta_{\mathbf{k}\mathbf{k}'}\,\delta_{m_c m_c'}\,\delta_{m_v m_v'} \\ &\quad - \delta_{m_c m_c'}\,\delta_{m_v m_v'} W(\,cv\mathbf{k}m_c m_v|c'v'\mathbf{k}'m_c m_v) \\ &\quad + \delta_{m_c m_v}\,\delta_{m_c' m_v'}\bar{v}(\,cv\mathbf{k}m_c m_c|c'v'\mathbf{k}'m_c' m_c') \end{aligned} \tag{36}$$

comprises three contributions. First, the diagonal part given by the differences of the QP eigenvalues in conduction and valence bands according to Eq. (31) describes the excitation of noninteracting quasielectrons and quasiholes. Second, the Hamiltonian includes the matrix elements of the statically screened Coulomb potential

$$\begin{aligned} W(\,cv\mathbf{k}m_c m_v|c'v'\mathbf{k}'m_c m_v) &= \int d\mathbf{r} \int d\mathbf{r}'\; \varphi_{c\mathbf{k}}^{*m_c}(\mathbf{r})\varphi_{c'\mathbf{k}'}^{m_c}(\mathbf{r}) W(\mathbf{r},\mathbf{r}')\varphi_{v\mathbf{k}}^{m_v}(\mathbf{r}')\varphi_{v'\mathbf{k}'}^{*m_v}(\mathbf{r}'), \end{aligned} \tag{37}$$

which describe the attractive interaction between electrons and holes. The third contribution to the excitonic Hamiltonian arises from the truncated bare Coulomb potential

$$\begin{aligned} \bar{v}(\,cv\mathbf{k}m_c m_c|c'v'\mathbf{k}'m_c' m_c') &= \int d\mathbf{r} \int d\mathbf{r}'\; \varphi_{c\mathbf{k}}^{*m_c}(\mathbf{r})\varphi_{v\mathbf{k}}^{m_c}(\mathbf{r})\bar{v}(\mathbf{r}-\mathbf{r}')\varphi_{c'\mathbf{k}'}^{m_c'}(\mathbf{r}')\varphi_{v'\mathbf{k}'}^{*m_c'}(\mathbf{r}'), \end{aligned} \tag{38}$$

which accounts for LFEs.

It is worthwhile to examine the spin structure of the resulting two-particle Hamiltonian more detailed. If one writes down H_{exc} in two-particle spin space which is spanned by the products of electron and hole one-particle spins and thereby omits orbital dependencies, one finds

$$H_{exc} = \begin{pmatrix} (E_c^\uparrow - E_v^\uparrow) - W^{\uparrow\uparrow} + \bar{v}^{\uparrow\uparrow} & 0 & 0 & \bar{v}^{\uparrow\downarrow} \\ 0 & (E_c^\uparrow - E_v^\downarrow) - W^{\uparrow\downarrow} & 0 & 0 \\ 0 & 0 & (E_c^\downarrow - E_v^\uparrow) - W^{\downarrow\uparrow} & 0 \\ \bar{v}^{\downarrow\uparrow} & 0 & 0 & (E_c^\downarrow - E_v^\downarrow) - W^{\downarrow\downarrow} + \bar{v}^{\downarrow\downarrow} \end{pmatrix} \begin{matrix} (m_c=\uparrow\, m_v=\uparrow) \\ (m_c=\uparrow\, m_v=\downarrow) \\ (m_c=\downarrow\, m_v=\uparrow) \\ (m_c=\downarrow\, m_v=\downarrow) \end{matrix}. \tag{39}$$

In the non-spin-polarized case it is common practice to diagonalize this Hamiltonian in spin space by utilizing singlet and triplet pair states instead of products of one-particle spins as basis sets. Consequently, the singlet and the three triplet contributions can be treated independently. Due to selection rules, it turns out that only the singlet contribution is relevant for the calculation of optical spectra. Thus, the rank of the BSE Hamiltonian can be reduced by a factor of 4 and it is sufficient to solve the eigenvalue problem of $H_{exc}=(E_c-E_v)-W+2\bar{v}$ in the singlet subspace.

If spin polarization is present, the two-particle problem becomes more complex. In contrast to the non-spin-polarized case the interaction matrix elements and QP eigenvalues depend explicitly on the one-particle spin quantum numbers. That is why it is futile to perform a basis change to singlet and triplet states as the pair spin quantum number is no longer well defined. However, Eq. (26) for the dielectric function shows that, due to the optical selection rules, it suffices to solve the eigenvalue problem in the subspace which is determined by $m_c=m_v$. The corresponding submatrix of the excitonic Hamiltonian (39), which is decoupled from the rest of the matrix, is spanned by the single-particle transitions with one and the same spin quantum number in the valence and conduction band $|v\mathbf{k}m\rangle \rightarrow |c\mathbf{k}m\rangle$; i.e., no spin flips occur. Consequently, the rank of the excitonic eigenvalue problem for the calculation of the optical response can be decreased by a factor of 2 in comparison to the eigenvalue problem (34). Exploiting this observation we obtain for the macroscopic dielectric function

$$\varepsilon_{mac}^{\alpha\alpha}(\omega) = 1 + \frac{1}{\Omega}\frac{e^2\hbar^2}{\varepsilon_0 m_0^2}\sum_{\Lambda} \times \left| \sum_{cv\mathbf{k}m} \frac{\langle c\mathbf{k}m|p_\alpha|v\mathbf{k}m\rangle^*}{\varepsilon_{c\mathbf{k}}^m - \varepsilon_{v\mathbf{k}}^m} A_\Lambda\left(\begin{smallmatrix} c\mathbf{k}\ v\mathbf{k} \\ m\ m \end{smallmatrix}\right) \right|^2 \times \sum_{\beta=\pm 1} \frac{1}{E_\Lambda - \beta\hbar(\omega + i\gamma)}, \tag{40}$$

whereas the transition energies E_Λ and the contributions $A_\Lambda(\begin{smallmatrix} c\mathbf{k}\ v\mathbf{k} \\ m\ m \end{smallmatrix})$ of a certain single-particle transition are determined as solutions of the reduced eigenvalue problem,

$$\sum_{c'v'\mathbf{k}'m'} H_{exc}\left(\begin{smallmatrix} c\mathbf{k}\ v\mathbf{k} \\ m\ m \end{smallmatrix} \middle| \begin{smallmatrix} c'\mathbf{k}'\ v'\mathbf{k}' \\ m'\ m' \end{smallmatrix}\right) A_\Lambda\left(\begin{smallmatrix} c'\mathbf{k}'\ v'\mathbf{k}' \\ m'\ m' \end{smallmatrix}\right) = E_\Lambda A_\Lambda\left(\begin{smallmatrix} c\mathbf{k}\ v\mathbf{k} \\ m\ m \end{smallmatrix}\right), \tag{41}$$

in which only pair amplitudes A_Λ diagonal in the spin quantum number appear.

III. GEOMETRY AND ELECTRONIC STRUCTURE: NUMERICAL APPROXIMATIONS AND RESULTS

A. Ground state

In order to compute total energies, magnetization and electron densities we start with the spin-polarized DFT-GGA implementation in the Vienna *ab initio* simulation package (VASP).[45] The pseudopotentials are generated by means of the projector-augmented-wave (PAW) method[46] that allows for the accurate treatment of the Mn $3d$, Mn $4s$, O $2s$, and O $2p$ valence electrons. In the region between the atomic cores the wave functions are expanded in plane waves up to a cutoff energy of 315 eV. The XC functional is parametrized as proposed by Perdew and Wang.[47,48] For intermediate spin polarizations we use the interpolation proposed by von Barth and Hedin.[49] For the ground-state calculations the BZ is sampled with a mesh of $8\times8\times8$ Monkhorst-Pack **k** points[50] corresponding to 60 **k** points in the irreducible wedge of the zone.

The minimization of total energy with respect to the atomic geometry and the arrangement of the Mn spins leads to a type-II antiferromagnetic (AFII) insulator that crystallizes in a rhombohedrally distorted rocksalt structure with a nominal lattice constant of 8.87 Å for the conventional magnetic cell. We find $B=146$ GPa for the isothermal bulk modulus and $B'=4.0$ for its pressure derivative. The rhombohedral distortion takes the form of a compression along the [111] direction with a distortion angle $\alpha=1.7°$ with respect to the cubic unit cell. The local magnetic moment at the Mn atoms amounts to $\mu=4.3\mu_B$. These results are in good agreement with neutron diffraction experiments[51,52] below the Néel temperature of $T_N=118$ K and other DFT-GGA calculations.[29,53]

B. Electronic band structure

The ground-state calculations yield a KS band structure for antiferromagnetic MnO [see Fig. 1(a)] which exhibits the most important features observed also in previous theoretical studies.[17] The uppermost valence bands are dominated by fairly flat e_g and t_{2g} bands derived from Mn $3d$ states. At values of about 3–7 eV below the valence-band maximum (VBM), which is located at the T point in the BZ, the O $2p$ bands with a rather strong dispersion occur. The lowest conduction band is a dispersive band with mainly Mn $4s$ character around its minimum at Γ. The higher unoccupied bands are dominated by empty Mn $3d$ levels. Characteristic direct and indirect gap values as well as the band splitting Δ_v between the occupied e_g and t_{2g} levels at Γ are listed in Table I. They clearly indicate the typical underestimation of band gaps by the eigenvalues of a DFT calculation using local or semilocal XC functionals.[41,42] The experimental gap measured by optical absorption[54] and photoconductivity[55] amounts to 3.6–3.8 eV and 3.8–4.2 eV, respectively. Combination of x-ray photoemission (XPS) data and bremsstrahlung-isochromat spectroscopy[56] (BIS) leads to a gap of about 3.9 ± 0.4 eV. The measured distance Δ_v between the valence-band e_g and t_{2g} levels is about 1.9 eV according to Ref. 56. Computations applying the nonlocal PBE0 XC functional[30] give rise to the larger value of 4.02 eV for the fundamental gap. We have utilized the spatially nonlocal HSE03 (Ref. 40) XC functional to obtain KS energies closer to the QP band structure [see Fig. 1(b)]. The calculated band structure and density of states (DOS) are similar to the PBE0 results in Ref. 30.

Despite the gap openings due to the nonlocality of the XC potential in PBE0 and HSE03, QP corrections are still missing. Recently, Faleev *et al.*[19] presented a band structure for MnO applying a new kind of self-consistent (SC) *GW* ap-

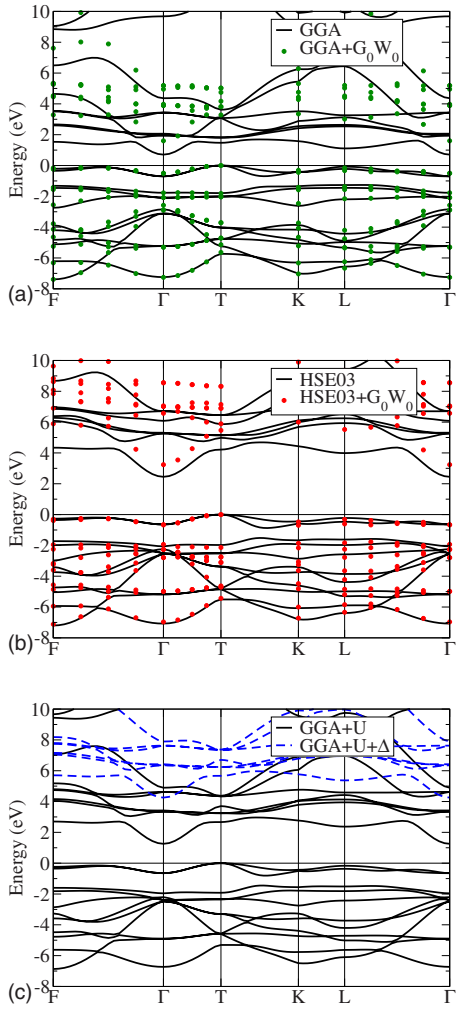

FIG. 1. (Color online) Band structures for MnO based on the GGA (a), HSE03 (b), and GGA+U (c) approaches (black lines). The corresponding QP energies in G_0W_0 are plotted as green dots (a) and red dots (b). In (c) the blue dashed lines indicate the scissors-shifted conduction bands. The VBM is set to zero in all plots.

proximation based on the all-electron, full-potential linear muffin-tin orbital method. Their results may be considered as a benchmark. In principle, the QP equation (30) has to be solved self-consistently, but this procedure is computationally extremely demanding. Therefore, we adopt the prevailing G_0W_0 approximation—i.e., the application of one-shot perturbation theory on top of a starting electronic structure from a DFT calculation. This approach is obviously most justified in the cases where the DFT starting point is close to the final QP result. It has been shown[57] that DFT calculations with HSE03 potentials yield such good starting points which can be successfully combined with a G_0W_0 calculation leading to gaps and shallow d-electron binding energies for semiconductors and insulators in good agreement with experimental results. As can be seen from Fig. 1 and Table I the QP corrections which are calculated within the PAW framework[58] still open the fundamental gaps substantially. The G_0W_0 calculations were performed using an $8\times8\times8$ **k**-point mesh including the Γ point and 150 bands for an

TABLE I. Direct and indirect gaps (the corresponding high-symmetry points in the BZ are indicated) and the e_g-t_{2g} splitting Δ_v of the valence bands at the Γ point. All values in eV.

Method	Indirect gap	Direct gap		Δ_v
	$T\rightarrow\Gamma$	$\Gamma\rightarrow\Gamma$	$L\rightarrow L$	
GGA	0.7	1.4	1.2	1.3
HSE03	2.5	3.1	4.2	1.7
GGA+U	1.3	1.9	2.5	1.6
GGA+G_0W_0	1.6	2.1	3.2	1.5
HSE03+G_0W_0	3.2	3.9	5.8	2.0
GGA+U+Δ	4.3	4.9	5.5	1.6

appropriate description of the screening function.

Examining the computed band structures in more detail one can see that all performed calculations yield an indirect insulator with a fundamental gap between the VBM at T and the conduction-band minimum (CBM) at Γ. As already mentioned, the GGA and GGA+G_0W_0 with gaps of 0.7 eV and 1.6 eV, respectively, severely underestimate the experimental values. One might argue that the underestimation of the gap in the GGA could be corrected by a scissors shift in the calculation of optical properties. But such an approach fails due to another deficiency of the DFT-GGA which predicts the lowest direct gap at L, whereas the HSE03 and G_0W_0 calculations as well as results from the literature[19,30] agree about the position of the lowest direct gap at Γ. Hence, in the case of MnO the GGA represents a bad starting point for the calculation of optical properties, where the transitions near the direct gap are important for the properties of the absorption onset.

The HSE03 approach overcomes most of the above-mentioned deficiencies [cf. Fig. 1(b) and Table I]. It yields 2.5 eV and 3.1 eV for the lowest indirect and direct gaps, respectively. These values are already sufficiently close to experimental results to justify the perturbational treatment of the GWA which results in 3.2 eV and 3.9 eV for the indirect and direct gaps in good agreement with the experimental values. In Fig. 2 the DOS computed in the HSE03+G_0W_0 approach is compared to results from XPS and BIS measurements.[56] The main features of the DOS—i.e., the position of the Mn 3d bands and the gap—can be reproduced in good agreement with the experimental data.

The drawback of this approach is that HSE03 and HSE03+G_0W_0 calculations are extremely time consuming and cannot be carried out for the large number of **k** points which is required for the computation of the excitonic matrix (36). Therefore, we have to find a way to obtain a band structure with less computational cost. We compute QP eigenvalues and wave functions in a simplified scheme, while the more sophisticated HSE03+G_0W_0 results serve as a benchmark. In a first step we apply the GGA+U method[32] in the approach of Dudarev *et al.*[59] where only the difference between the on-site Coulomb interaction and the exchange parameter, $U-J$, determines the band structure. A value $U-J=2.0$ eV yields a good fit for the valence band positions obtained in the HSE03+G_0W_0 framework. Larger values of

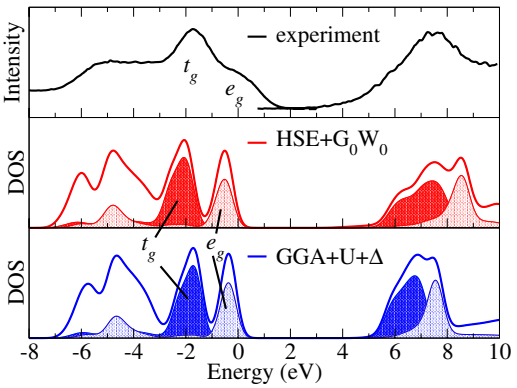

FIG. 2. (Color online) DOS and partial DOS (projected on t_{2g} and e_g levels) for MnO computed within HSE03+G_0W_0 (red line) and GGA+U+Δ with U=2.0 eV and a scissors shift Δ=3.0 eV (blue line) in comparison with the experimental XPS+BIS measurements (upper panel) from Ref. 56. The calculated spectra are broadened by convolution with a Gaussian with 0.6 eV full width at half maximum. For the computed curves the VBM is set to zero while the t_{2g} peak of the experiment is aligned with the t_{2g} peak in the GGA+U+Δ DOS.

about 6–7 eV as predicted in the literature[30,32,60] shift down the occupied Mn 3*d* bands too much. They do not open the gap significantly, since the CBM at Γ shows *s*-like character and the VBM is no longer dominated by Mn 3*d* states for larger values of U and, therefore, scarcely affected by the additional potential.

Whereas the fit for the valence bands in GGA+U is quite good, the fundamental gap is still severely underestimated [see Fig. 1(c) and Table I]. Approximate QP corrections can be obtained by an additional scissors shift Δ to account for the remaining gap underestimation. A value Δ=3.0 eV is chosen such that the obtained DOS shows reasonable agreement with the measured curve and the HSE03+G_0W_0 result (see Fig. 2). Especially the characteristic peaks which arise from the t_{2g} and e_g states in the occupied and empty bands can be well reproduced; only the width of the conduction bands is slightly underestimated. The main deficiency of the GGA+U+Δ approach is the lower dispersion of the first conduction band in comparison to HSE03+G_0W_0, resulting in larger indirect and direct gaps. However, this effect has almost no influence on the DOS (cf. Fig. 2) and the joint DOS, since both are comparably small in the respective energy region. Consequently, we conclude that the GGA+U+Δ approach may be utilized as a starting point for the computations of optical properties and excitonic effects despite a slight shift of the absorption edge toward higher energies.

IV. DIELECTRIC FUNCTION AND EXCITONIC EFFECTS

A. Computation of optical spectra

For the evaluation of optical spectra a mesh of $10\times10\times10$ Monkhorst-Pack **k** points is used to sample the BZ. The **k** mesh is shifted by $0.2\times0.3\times0.5$ fractions of the distance between two adjacent **k** points, thus avoiding spurious effects from high-symmetry points and taking into account more symmetry-inequivalent **k** points. This procedure results in a denser energy sampling of the optical spectra. In addition to the pair energies of noninteracting quasielectrons and quasiholes the calculation of the excitonic Hamiltonian (36) requires the computation of Coulomb matrix elements. The dielectric function for the matrix elements of W in the Hamiltonian is described using a model screening function,[61] which is fully determined by the electron density in the system and the static electronic dielectric constant. The value ε_∞=4.95 for the latter has been taken from measurements.[62,63] The number of pair states in the spin-polarized excitonic Hamiltonian is determined by $2N_c\times N_v\times N_{\mathbf{k}}$ with N_c the number of conduction bands, N_v the number of valence bands, and $N_{\mathbf{k}}$ the number of **k** points. As explained in more detail above, the factor of 2 is a consequence of the inclusion of collinear magnetism. We restrict the size of the matrix by means of an energy cutoff; i.e., we include all electron-hole pairs with GGA+U transition energies below this cutoff.

Optical spectra are obtained from the excitonic Hamiltonian in two different ways. In order to discuss oscillator strengths and excitonic wave functions of interesting electron-hole pairs, the eigenvalue problem is solved by a diagonalization of the pair Hamiltonian. For the calculation of optical spectra in an extended frequency range a huge number of pair states, typically between 50 000 and 100 000, is required. As it is not possible to diagonalize matrices of this size due to computational costs, the time-development scheme introduced by Schmidt *et al.*[64] is applied. Due to its quadratic scaling, this method reduces the computational effort significantly and yields the dielectric function directly without explicitly evaluating the eigenvalues and eigenvectors of the excitonic Hamiltonian.

B. Optical properties

The rhombohedral distortion of the rocksalt structure and the magnetic ordering along the [111] direction in antiferromagnetic MnO give rise to a macroscopic anisotropy. Due to this effect, deviations from cubic symmetry should occur. However, they are extremely small and their study requires an accuracy which is beyond that of the applied methods. Therefore, the anisotropy is omitted and only the trace of the dielectric tensor is studied. This is in agreement with the experiments[54,65,66] in which no anisotropy has been resolved.

The average dielectric function in the independent-quasiparticle approximation,[67] more precisely in the RPA, but with the scissors shift already included, is plotted in Fig. 3. In the inset the imaginary part is divided into contributions from different optical transitions. We have distinguished three groups of initial valence bands according to the orbital symmetry of the mainly contributing states: the two highest valence bands with mainly Mn 3*d* e_g character, the three Mn 3*d* t_{2g} bands, and finally the transitions from the more dispersive valence bands at lower energies. The related optical transitions explain the peak structure of the imaginary part of the dielectric function shown in Fig. 3. The lowest peak at about 6.0 eV is clearly related to optical transitions from Mn

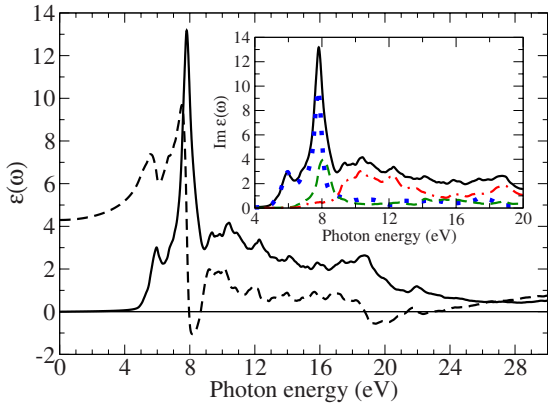

FIG. 3. (Color online) Real (dashed line) and imaginary (solid line) part of the dielectric function $\varepsilon(\omega)$ calculated in independent-quasiparticle approximation (GGA+U+Δ) versus photon energy $\hbar\omega$. In the inset the absorption spectrum (black solid line) is divided into contributions from initial states in the two highest valence bands with e_g character (blue dotted line), the three t_{2g} valence bands (green dashed line), and the lower dispersive valence bands (red dash-dotted line).

$3d$ e_g states into conduction bands. However, these transitions also yield significant contributions to the main peak at a photon energy of 7.8 eV. The latter is also affected by the transitions from the occupied Mn $3d$ t_{2g} bands. The high-energy region above 9 eV is essentially related to optical transitions from the lower dispersive valence bands which include the O $2p$ states.

In Fig. 4 the imaginary part of the dielectric function in the independent-quasiparticle approximation is compared with the results from a calculation including the screened electron-hole attraction and local-field effects using a Lorentzian broadening of 0.1 eV and an energy cutoff of 7.5 eV. We find the same general tendencies which have been discussed for the optical absorption of many semiconductors and insulators before.[9–11,64,68] The inclusion of the electron-hole attraction yields a significant redshift of the absorption spectrum which amounts to approximately 0.8 eV in the case of

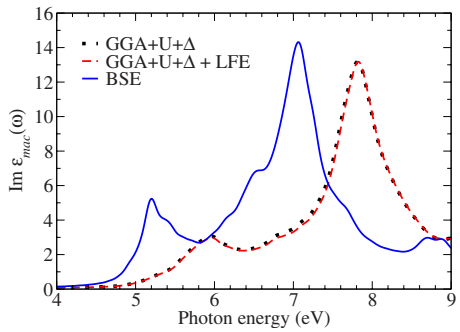

FIG. 4. (Color online) Imaginary part of the dielectric function $\varepsilon(\omega)$ versus photon energy $\hbar\omega$. The spectra are calculated on different levels of approximation: independent quasiparticles in the GGA+U+Δ approach with (red dashed line) and without (black dotted line) LFEs, interacting quasiparticles by solving the BSE with electron-hole attraction and LFEs (blue solid line).

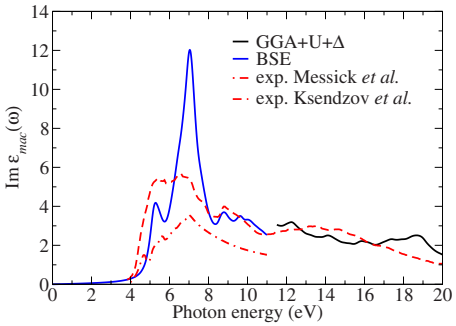

FIG. 5. (Color online) Comparison of calculated and measured absorption spectra. The low-energy part of the calculated curve which includes excitonic effects (blue solid line) is continued by the spectrum in independent-quasiparticle approximation (black solid line). Experimental data are taken from Messick *et al.* (Ref. 65) (red dot-dashed line) and Ksendzov *et al.* (Ref. 66) (red dashed line).

MnO. Furthermore, a redistribution of spectral weight to lower photon energies is observable. In particular, the oscillator strength of the first peak at 5.2 eV almost doubles in comparison to the independent-quasiparticle calculation and an additional shoulder at 5.4 eV appears. A new feature that emerges in the excitonic calculation is a shoulder at 6.6 eV below the strongest peak at 7.1 eV. In the case of MnO the influence of the LFEs on the imaginary part of the dielectric function turns out to be almost negligible. In comparison to semiconductors like Si[5,9] the LFEs are much weaker for two reasons. First, the matrix elements of $\bar{v}$ are significantly smaller due to a stronger localization and lower overlap of the contributing wave functions. Second, according to Eq. (38) the electron-hole exchange can only occur between electrons and holes with the same spin quantum number, which are localized at Mn atoms with different spin orientations and, hence, at least in second-nearest-neighbor distance.

For the computation of an optical spectrum with excitonic effects in a wide energy range, which can be compared to the experimental results of Messick *et al.*[65] and Ksendzov *et al.*[66] (see Fig. 5), the number of **k** points is reduced to 512 in the full BZ, thus enabling the use of a larger cutoff energy of 12.0 eV for the contributing noninteracting electron-hole pairs. The curve in Fig. 5 is broadened by γ=0.2 eV. Due to the reduced number of **k** points and the larger broadening, the shoulder at 6.6 eV is not resolved. Comparing with measurements one first has to note that the available experimental data differ significantly, as is shown in Fig. 5. In the energy range below 7 eV, Refs. 65 and 66 agree about the positions of the reflectance peaks, but significant discrepancies are reported for the oscillator strengths in the imaginary part of the dielectric function. Concerning the main features of the spectrum, the calculated curve for Im $\varepsilon_{mac}(\omega)$ agrees with the findings of Ref. 66: We find two pronounced peaks at 5.3 eV and 7 eV matching the positions of the maxima of the experimental curve. The relative oscillator strength of these peaks differs from the intensity ratio obtained by Ksendzov *et al.*; i.e., the second peak is much stronger in the calculated spectrum. In the energy range between 8 eV and 11 eV the measured values can be reproduced. For higher photon energies a BSE treatment is not possible due to memory restrictions.

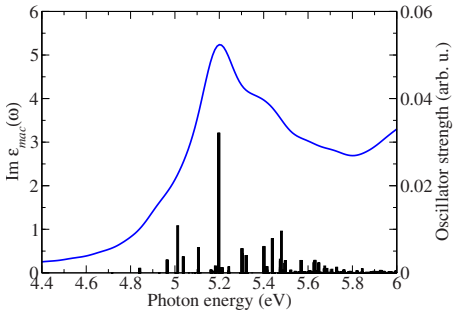

FIG. 6. (Color online) Imaginary part of the macroscopic dielectric function $\varepsilon_{mac}(\omega)$ (blue line) and oscillator strengths (black bars) versus the respective pair-excitation energies in the low-energy range of the spectrum.

In the literature several references[54,69–71] can be found which report about optical transitions below the fundamental gap. It is argued[69] that these transitions are related to intra-atomic spin-flip *d*-*d* excitations between the valence and conduction states of one and the same Mn atom. As the optical selection rules in the absence of spin-orbit coupling do not allow for such transitions, they cannot be observed in the computed spectra.

C. Interplay of excitonic and spin effects

The most remarkable new feature in the absorption spectrum with excitonic effects is the above-mentioned enhancement of the peak at 5.2 eV. In order to understand its origin we examine the oscillator strengths of the excitonic transitions that contribute to the absorption spectrum in that region. For the calculations we use a refined unshifted **k**-point mesh of $12\times12\times12$ points in the BZ and include only the two highest occupied bands and the lowest empty band in the excitonic Hamiltonian. In Fig. 6 the computed oscillator strengths, obtained by direct diagonalization of the Hamiltonian, are plotted versus the corresponding pair excitation energies. For comparison the calculated optical absorption from Fig. 4 is also given. It can be seen that the appearance of the peak is clearly related to an excitonic resonance state with a comparatively large oscillator strength.

In the following we analyze the excitonic two-particle wave function for this specific resonance state. The two-particle wave function for fixed one-particle spin *m* is defined by

$$A^m_\Lambda(\mathbf{r},\mathbf{r}') = \sum_{cv\mathbf{k}} A_\Lambda\binom{c\mathbf{k}\ v\mathbf{k}}{m\ \ m}\varphi^m_{c\mathbf{k}}(\mathbf{r})\varphi^{*m}_{v\mathbf{k}}(\mathbf{r}'), \tag{42}$$

whereas the coordinate **r** refers to the position of the electron and $\mathbf{r}'$ to that of the hole. We fix the hole at a Mn atom whose spin-up 3*d* orbitals are occupied and compute the corresponding spin-resolved density distribution of the electron according to

$$\rho^m_\Lambda(\mathbf{r},\mathbf{r}') = |A^m_\Lambda(\mathbf{r},\mathbf{r}')|^2 \tag{43}$$

for the resonance state (see Fig. 7). As is visible in Fig. 7, the spin-up electron is located mainly in the vicinity of Mn atoms with occupied 3*d* spin-down orbitals. This behavior can be understood by means of the spin selection rule for dipole-allowed optical transitions: An electron from a spin-up orbital can only be excited in empty spin-up orbitals. The latter are located at the Mn atoms whose spin-down orbitals are filled. Consequently, the density of the spin-up excitonic wave function is high at the Mn atoms with filled spin-down orbitals and very low around the conversely occupied Mn atoms. This supports the picture of the dominance of interatomic transitions in the interband region of the absorption spectrum and shows the importance of the consideration of spin-polarization effects for the calculation of optical spectra of magnetic systems.

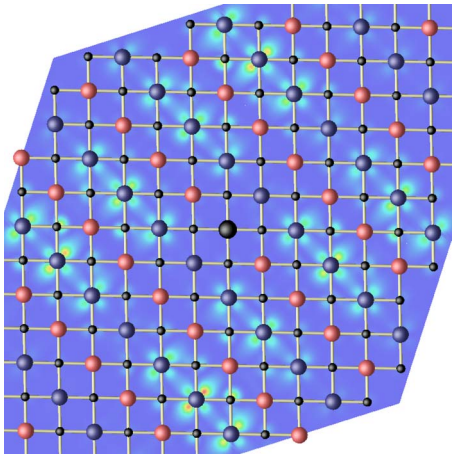

FIG. 7. (Color online) Spin-up density distribution of the excitonic wave function in the (001) plane for the resonance state at 5.2 eV. Light red balls represent Mn atoms with occupied 3*d* spin-up orbitals and dark blue balls their counterparts with filled 3*d* spin-down orbitals. Oxygen atoms are denoted by small black spheres, while the position of the hole is indicated by the large black ball in the center.

V. SUMMARY AND CONCLUSIONS

In conclusion, we have derived the Dyson and Bethe-Salpeter equation for a spin-polarized system with noncollinear or collinear spins. The explicit calculations have been performed for the paradigmatic example of antiferromagnetic MnO within Hedin's *GW* approach and the restriction to collinearity. The QP self-energy is diagonal with respect to the spin quantum number and, therefore, only shifts the KS energy of a one-particle state with defined spin. Because of the strong localization of the Mn 3*d* states, the description of the KS states in a (semi)local approach represents a bad starting point for a subsequent QP calculation in first-order perturbation theory. As an improved starting point, we have used a spatially nonlocal XC functional in the KS equation. The resulting QP picture correctly describes the band structure, including details of the conduction and valence bands.

The spin influence is much more drastic for the two-particle excitations which are relevant for the calculation of optical properties. The spin polarization in the system modifies the screened Coulomb attraction between electrons and

holes as well as the electron-hole exchange via the spatial parts of the one-particle wave functions. The separation of singlet and triplet states in the excitonic two-particle Hamiltonian no longer holds for magnetic systems. In order to account for the huge number of contributing electron-hole pairs, the QP energies and wave functions are approximated by those obtained within the GGA+U scheme with QP shifts from a scissors operator approach. The optical absorption spectrum of MnO is remarkably influenced by the many-body effects. The inclusion of the interaction terms yields a significant overall redshift of the spectrum as well as a redistribution of spectral weight to lower energies. The influence of LFEs is small due to the antiferromagnetic ordering. It has been shown that it is important to take spin effects into account to explain the character of the interatomic transitions between Mn atoms with reversely oriented spins. The distribution of the electron-hole pair wave function clearly reveals the spin ordering in the antiferromagnetic system.

ACKNOWLEDGMENTS

We thank Patrick H. Hahn for valuable discussions. This work was supported by the European Community in the framework of the network of excellence NANOQUANTA (Contract No. NMP4-CT-2004-500198) and the Deutsche Forschungsgemeinschaft (Project No. Be 1346/18-2 and Be 1346/20–1).

[1] G. Onida, L. Reining, and A. Rubio, Rev. Mod. Phys. **74**, 601 (2002).
[2] L. Hedin, Phys. Rev. **139**, A796 (1965).
[3] L. Hedin and S. Lundqvist, in *Solid State Physics: Advances in Research and Applications*, edited by F. Seitz, D. Turnbull, and H. Ehrenreich (Academic Press, New York, 1969), Vol. 23, p. 1.
[4] L. J. Sham and T. M. Rice, Phys. Rev. **144**, 708 (1966).
[5] W. Hanke and L. J. Sham, Phys. Rev. Lett. **43**, 387 (1979).
[6] W. Hanke and L. J. Sham, Phys. Rev. B **21**, 4656 (1980).
[7] G. Strinati, Riv. Nuovo Cimento **11**, 1 (1988).
[8] M. Rohlfing and S. G. Louie, Phys. Rev. B **62**, 4927 (2000).
[9] S. Albrecht, L. Reining, R. Del Sole, and G. Onida, Phys. Rev. Lett. **80**, 4510 (1998).
[10] L. X. Benedict, E. L. Shirley, and R. B. Bohn, Phys. Rev. Lett. **80**, 4514 (1998).
[11] M. Rohlfing and S. G. Louie, Phys. Rev. Lett. **81**, 2312 (1998).
[12] M. Rohlfing and S. G. Louie, Phys. Rev. Lett. **83**, 856 (1999).
[13] P. H. Hahn, W. G. Schmidt, and F. Bechstedt, Phys. Rev. Lett. **88**, 016402 (2001).
[14] M. Rohlfing and S. G. Louie, Phys. Rev. Lett. **82**, 1959 (1999).
[15] P. H. Hahn, W. G. Schmidt, K. Seino, M. Preuss, F. Bechstedt, and J. Bernholc, Phys. Rev. Lett. **94**, 037404 (2005).
[16] P. H. Hahn, W. G. Schmidt, and F. Bechstedt, Phys. Rev. B **72**, 245425 (2005).
[17] K. Terakura, T. Oguchi, A. R. Williams, and J. Kübler, Phys. Rev. B **30**, 4734 (1984).
[18] V. I. Anisimov, I. V. Solovyev, M. A. Korotin, M. T. Czyżyk, and G. A. Sawatzky, Phys. Rev. B **48**, 16929 (1993).
[19] S. V. Faleev, M. van Schilfgaarde, and T. Kotani, Phys. Rev. Lett. **93**, 126406 (2004).
[20] M. Marques, L. K. Teles, L. M. R. Scolfaro, J. Furthmüller, F. Bechstedt, and L. G. Ferreira, Appl. Phys. Lett. **86**, 164105 (2005).
[21] M. Marques, L. M. R. Scolfaro, L. K. Teles, J. Furthmüller, F. Bechstedt, and L. G. Ferreira, Appl. Phys. Lett. **88**, 022507 (2006).
[22] G. A. Prinz, Science **282**, 1660 (1998).
[23] H. Ohno, A. Shen, F. Matsukura, A. Oiwa, A. Endo, S. Katsumoto, and Y. Iye, Appl. Phys. Lett. **69**, 363 (1996).
[24] T. Dietl, H. Ohno, F. Matsukura, J. Cibert, and D. Ferrand, Science **287**, 1019 (2000).
[25] P. Segovia, D. Purdie, M. Hengsberger, and Y. Baer, Nature (London) **402**, 504 (1999).
[26] M. G. Zacher, E. Arrigoni, W. Hanke, and J. R. Schrieffer, Phys. Rev. B **57**, 6370 (1998).
[27] J. S. Wilson, A. S. Dhoot, A. J. A. B. Seeley, M. S. Khan, A. Köhler, and R. H. Friend, Nature (London) **413**, 828 (2001).
[28] R. W. Saalfrank, A. Scheurer, I. Bernt, F. W. Heinemann, A. V. Postnikov, V. Schünemann, A. X. Trautwein, M. S. Alam, H. Rupp, and P. Müller, Dalton Trans. **23**, 2865 (2006).
[29] J. E. Pask, D. J. Singh, I. I. Mazin, C. S. Hellberg, and J. Kortus, Phys. Rev. B **64**, 024403 (2001).
[30] C. Franchini, V. Bayer, R. Podloucky, J. Paier, and G. Kresse, Phys. Rev. B **72**, 045132 (2005).
[31] A. Svane and O. Gunnarsson, Phys. Rev. Lett. **65**, 1148 (1990).
[32] V. I. Anisimov, J. Zaanen, and O. K. Andersen, Phys. Rev. B **44**, 943 (1991).
[33] F. Aryasetiawan and O. Gunnarsson, Phys. Rev. Lett. **74**, 3221 (1995).
[34] S. Massidda, A. Continenza, M. Posternak, and A. Baldereschi, Phys. Rev. B **55**, 13494 (1997).
[35] J.-L. Li, G.-M. Rignanese, and S. G. Louie, Phys. Rev. B **71**, 193102 (2005).
[36] A. Georges, G. Kotliar, W. Krauth, and M. J. Rozenberg, Rev. Mod. Phys. **68**, 13 (1996).
[37] X. Ren, I. Leonov, G. Keller, M. Kollar, I. Nekrasov, and D. Vollhardt, Phys. Rev. B **74**, 195114 (2006).
[38] P. Hohenberg and W. Kohn, Phys. Rev. **136**, B864 (1964).
[39] W. Kohn and L. J. Sham, Phys. Rev. **140**, A1133 (1965).
[40] J. Heyd, G. E. Scuseria, and M. Ernzerhof, J. Chem. Phys. **118**, 8207 (2003).
[41] M. S. Hybertsen and S. G. Louie, Phys. Rev. B **34**, 5390 (1986).
[42] W. G. Aulbur, L. Jönsson, and J. W. Wilkins, in *Solid State Physics. Advances in Research and Applications*, edited by H. Ehrenreich and F. Spaepen (Academic Press, San Diego, 2000), Vol. 54, p. 1.
[43] S. L. Adler, Phys. Rev. **126**, 413 (1962).
[44] N. Wiser, Phys. Rev. **129**, 62 (1963).
[45] G. Kresse and J. Furthmüller, Comput. Mater. Sci. **6**, 15 (1996).
[46] G. Kresse and D. Joubert, Phys. Rev. B **59**, 1758 (1999).
[47] J. P. Perdew, in *Electronic Structure of Solids '91*, edited by P. Ziesche and H. Eschrig (Akademie-Verlag, Berlin, 1991), p. 11.

[48] J. P. Perdew and Y. Wang, Phys. Rev. B **45**, 13244 (1992).
[49] U. von Barth and L. Hedin, J. Phys. C **5**, 1629 (1972).
[50] H. J. Monkhorst and J. D. Pack, Phys. Rev. B **13**, 5188 (1976).
[51] A. K. Cheetham and D. A. O. Hope, Phys. Rev. B **27**, 6964 (1983).
[52] H. Shaked, J. Faber, Jr., and R. L. Hitterman, Phys. Rev. B **38**, 11901 (1988).
[53] P. Dufek, P. Blaha, V. Sliwko, and K. Schwarz, Phys. Rev. B **49**, 10170 (1994).
[54] R. N. Iskenderov, I. A. Drabkin, L. T. Emel'yanova, and Y. M. Ksendzov, Fiz. Tverd. Tela (Leningrad) **10**, 2573 (1968).
[55] I. A. Drabkin, L. T. Emel'yanova, R. N. Iskenderov, and Y. M. Ksendzov, Fiz. Tverd. Tela (Leningrad) **10**, 3082 (1968).
[56] J. van Elp, R. H. Potze, H. Eskes, R. Berger, and G. A. Sawatzky, Phys. Rev. B **44**, 1530 (1991).
[57] F. Fuchs, J. Furthmüller, F. Bechstedt, M. Shishkin, and G. Kresse, Phys. Rev. B **76**, 115109 (2007).
[58] M. Shishkin and G. Kresse, Phys. Rev. B **74**, 035101 (2006).
[59] S. L. Dudarev, G. A. Botton, S. Y. Savrasov, C. J. Humphreys, and A. P. Sutton, Phys. Rev. B **57**, 1505 (1998).
[60] I. V. Solovyev and K. Terakura, Phys. Rev. B **58**, 15496 (1998).
[61] J. Furthmüller, G. Cappellini, H.-C. Weissker, and F. Bechstedt, Phys. Rev. B **66**, 045110 (2002).
[62] J. N. Plendl, L. C. Mansur, S. S. Mitra, and I. F. Chang, Solid State Commun. **7**, 109 (1969).
[63] S. Mochizuki, J. Phys.: Condens. Matter **1**, 10351 (1989).
[64] W. G. Schmidt, S. Glutsch, P. H. Hahn, and F. Bechstedt, Phys. Rev. B **67**, 085307 (2003).
[65] L. Messick, W. C. Walker, and R. Glosser, Phys. Rev. B **6**, 3941 (1972).
[66] Y. M. Ksendzov, I. L. Korobova, K. K. Sidorin, and G. P. Startsev, Fiz. Tverd. Tela (Leningrad) **18**, 173 (1976).
[67] B. Adolph, V. I. Gavrilenko, K. Tenelsen, F. Bechstedt, and R. Del Sole, Phys. Rev. B **53**, 9797 (1996).
[68] F. Bechstedt, K. Seino, P. H. Hahn, and W. G. Schmidt, Phys. Rev. B **72**, 245114 (2005).
[69] G. W. Pratt, Jr. and R. Coelho, Phys. Rev. **116**, 281 (1959).
[70] D. R. Huffman, R. L. Wild, and M. Shinmei, J. Chem. Phys. **50**, 4092 (1969).
[71] H.-h. Chou and H. Y. Fan, Phys. Rev. B **10**, 901 (1974).